iScience

CellPress
OPEN ACCESS

Article

Simulated vestibular spatial disorientation mouse model under coupled rotation revealing potential involvement of Slc17a6

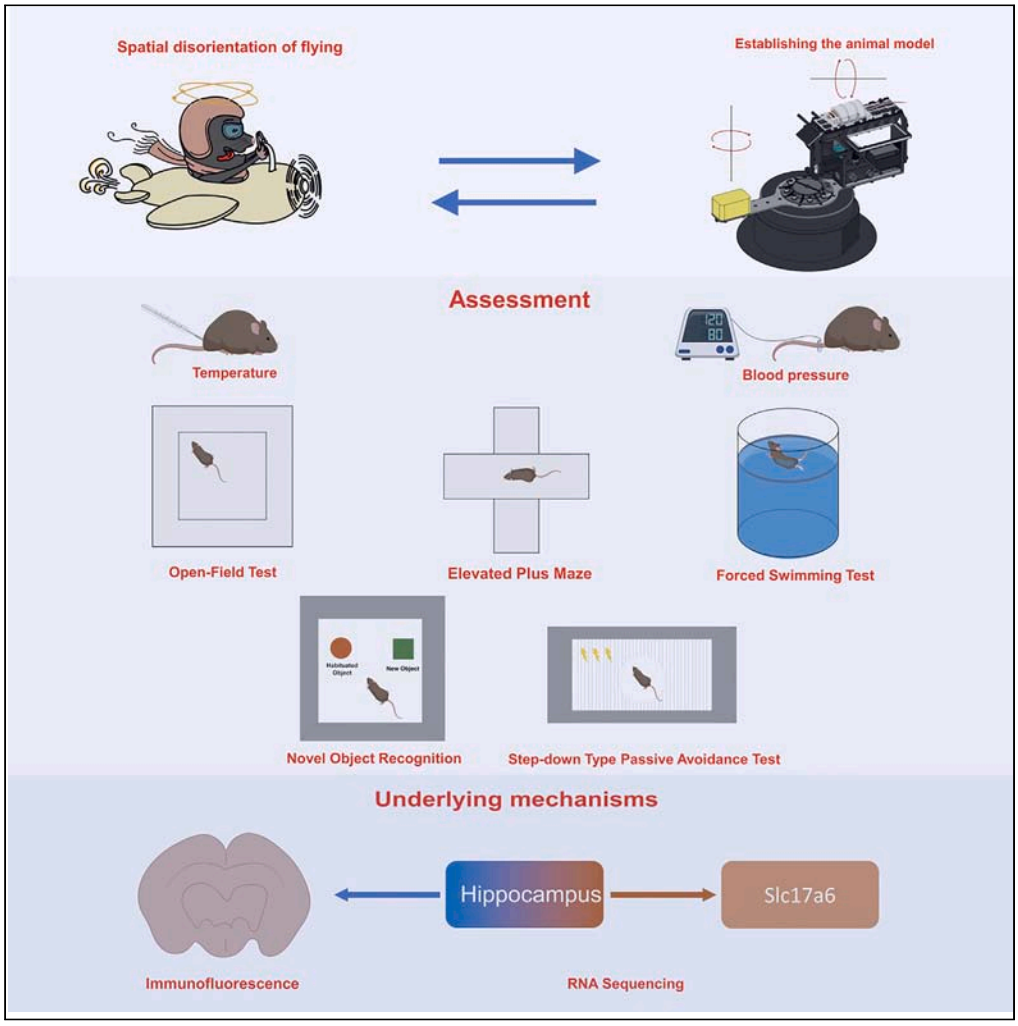

Tong Chang, Min Zhang, Jing Zhu, ..., Hao-tian Wang, Xiao-Cheng Wang, Yong Liu

wxcnose@126.com (X.-C.W.)
liuyong@fmmu.edu.cn (Y.L.)

Highlights

A groundbreaking approach to establish a murine model of vestibular spatial disorientation

An innovative method to assess a murine model of vestibular spatial disorientation

Spatial disorientation potentially linked to hippocampal neuronal hyperactivity

Spatial disorientation may be linked to reduced Slc17a6 expression

Chang et al., iScience 26, 108498
December 15, 2023
https://doi.org/10.1016/j.isci.2023.108498

iScience

CellPress
OPEN ACCESS

Article

Simulated vestibular spatial disorientation mouse model under coupled rotation revealing potential involvement of Slc17a6

Tong Chang,[1,2,5,6] Min Zhang,[1,2,5] Jing Zhu,[1,2,5] Han Wang,[1,2] Cong-cong Li,[1,2] Kan Wu,[1,2] Zhuo-ru Zhang,[1,2] Yi-hong Jiang,[1,2] Fei Wang,[3] Hao-tian Wang,[3] Xiao-Cheng Wang,[1,2,*] and Yong Liu[4,*]

SUMMARY

Spatial disorientation (SD) is the main contributor to flight safety risks, but research progress in animals has been limited, impeding a deeper understanding of the underlying mechanisms of SD. This study proposed a method for constructing and evaluating a vestibular SD mouse model, which adopted coupled rotational stimulation with visual occlusion. Physiological parameters were measured alongside behavioral indices to assess the model, and neuronal changes were observed through immunofluorescent staining. The evaluation of the model involved observing decreased colonic temperature and increased arterial blood pressure in mice exposed to SD, along with notable impairments in motor and cognitive function. Our investigation unveiled that vestibular SD stimulation elicited neuronal activation in spatially associated cerebral areas, such as the hippocampus. Furthermore, transcriptomic sequencing and bioinformatics analysis revealed the potential involvement of Slc17a6 in the mechanism of SD. These findings lay a foundation for further investigation into the molecular mechanisms underlying SD.

INTRODUCTION

Spatial disorientation (SD) is a multifaceted physiological and psychological phenomenon[1] that refers to the mismatch between perceived and actual spatial orientation. As a result of the stark contrast between three-dimensional aerial navigation and prolonged exposure to two-dimensional land-based activities, virtually every pilot will inevitably encounter SD during their aviation tenure.[2–4] Currently, SD simulation training is primarily conducted through piloting flight simulators to enhance the recognition ability and initiate the appropriate response to SD occurrences, thereby reducing the accident rate caused by SD[5,6]; however, the rate of progress of research on the mechanism of SD occurrence is slow. Thus, it is imperative to develop animal models that mimic typical SD-inducing scenarios and conduct research on the physiological and psychological states of the animals, as well as explore the underlying mechanisms of SD.

SD occurs due to the integration of perception and cognition,[7] with a crucial role played by the nervous system. Studies have indicated that rats can develop SD through various rotational or inversion techniques.[8–11] During this process, abnormal head direction cell discharges occur within the rat nervous system.[12] Exposure to such an environment can impair the hippocampus and medial entorhinal cortex (MEnt) function,[13] reducing the rats' ability to orient themselves. Previous research suggested that SD could be induced in experimental animals, particularly vestibular SD; the procedure involves uniaxial rotational stimuli to elicit somatogyral vestibular illusions. However, these methods have limitations in simulating SD, which manifests as a weak-intensity stimulus with a short duration. During flights, pilots frequently encounter more intricate and intense SD, including Coriolis illusions that result from biaxial coupled stimulation of their semicircular canals.[14,15] Unfortunately, improved aircraft performance leads linear and angular acceleration to appear simultaneously, making pilots more vulnerable to these complex forms of SD.[16]

Currently, there is a lack of suitable methodology for constructing and evaluating vestibular SD mouse models, resulting in difficulties while exploring the functional changes of neurons in related brain areas before and after the occurrence of SD. To address this knowledge gap, we induced distinct types of vestibular SD using a self-developed, dual-axis coupled motion device. We assessed physiological parameters, including rectal temperature and blood pressure, pre- and post-SD conditions, and examined mice's behavioral and cognitive alterations after stimulation. Furthermore, we explored the neural activation of nuclei clusters related to spatial orientation in areas such as the

[1]Center of Clinical Aerospace Medicine, School of Aerospace Medicine, Key Laboratory of Aerospace Medicine of Ministry of Education, Air Force Medical University, Xi'an 710032, China
[2]Department of Aviation Medicine, The First Affiliated Hospital, Air Force Medical University, Xi'an 710032, China
[3]School of Basic Medicine, Air Force Medical University, Xi'an 710032, China
[4]School of Aerospace Medicine, Key Laboratory of Aerospace Medicine of Ministry of Education, Air Force Medical University, Xi'an 710032, China
[5]These authors contributed equally
[6]Lead contact
*Correspondence: wxcnose@126.com (X.-C.W.), liuyong@fmmu.edu.cn (Y.L.)
https://doi.org/10.1016/j.isci.2023.108498

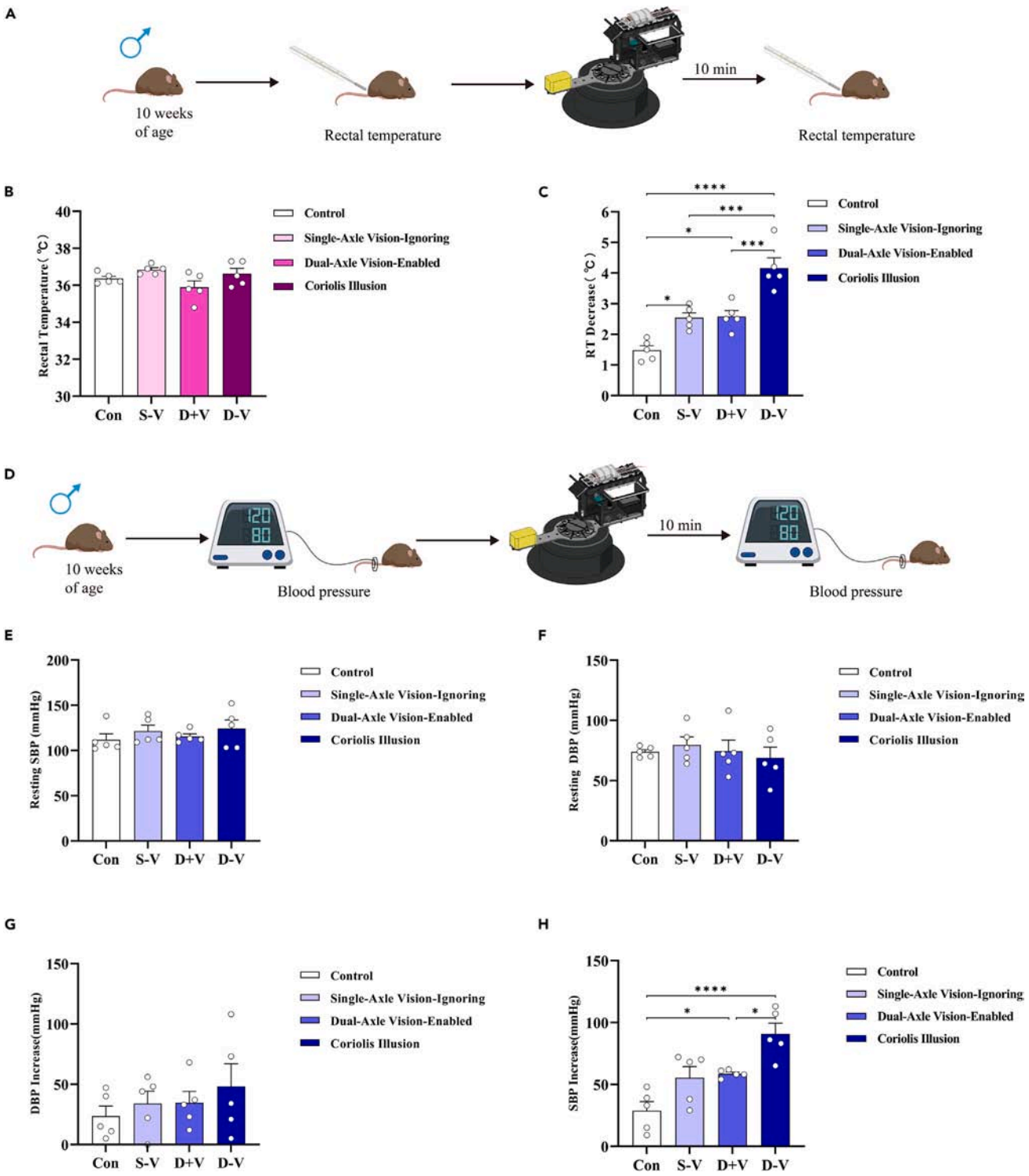

Figure 1. The effect of spatial disorientation on the physiological parameters in mice

(A) Experimental procedure.

(B) Before the stimulation, there was no significant difference in rectal temperature among the groups.

(C) Compared to the control group, the rectal temperature of the mice in each rotating group significantly decreased, with the Coriolis illusion group showing the most significant decrease.

(D) Experimental procedure.

Figure 1. *Continued*

(E) The baseline resting diastolic blood pressure of the mice before stimulation.

(F) The baseline resting systolic blood pressure of the mice before stimulation.

(G) The mouse groups did not show a significant difference in diastolic blood pressure changes following stimulation.

(H) The systolic blood pressure of two groups of mice subjected to biaxial rotation was significantly elevated compared to that of the control group, with a more pronounced increase in the Coriolis illusion group (n = 5 mice per group). Error bars represent ±standard error of the mean. *p < 0.05, ***p < 0.001, ****p < 0.0001. RT, rectal temperature.

hippocampus. In addition, by applying transcriptomic sequencing and bioinformatics techniques, we shed light on the potentially pivotal role of Slc17a6 in the occurrence of SD. In a broader sense, our research introduces a revolutionary approach for constructing and assessing vestibular SD mouse models while identifying genes associated with the onset of SD. Thus, our study establishes a firm groundwork for comprehending the intricate molecular mechanisms underlying SD.

RESULTS

SD results in decreasing rectal temperature in mice

Various groups of mice were stimulated with different axes' (Figures S1C–S1F) SD stimuli to investigate any changes in their body temperature. The rectal temperature of the mice was measured using a rectal thermometer before and after the stimulation (Figure 1A). The rectal temperatures of all groups were measured before stimulation to ensure there were no individual differences, and no significant differences were found ($p > 0.05$; Figure 1B). After exposure to the different stimuli, the rectal temperature of the mice decreased in all tested groups. In comparison to the control group, the rectal temperature of the mice was significantly reduced in each rotation stimulation group ($p < 0.05$; Figure 1C). The mice that underwent Coriolis illusion had a more significant decrease in their rectal temperature than the mice in the D + V group, who experienced the same biaxially coupled rotation but with their vision obscured ($p < 0.001$; Figure 1C). This decrease was also the most significant among all groups.

SD results in increased systolic blood pressure (SBP) in mice

Blood pressure was indirectly measured before and after stimulation (Figure 1D). The systolic blood pressure (SBP) in all groups increased after stimulation, with the biaxial rotation stimulation group showing a more significant increase compared to the control group ($p < 0.05$; Figure 1E). Additionally, the increase in the Coriolis illusion group with blocked vision was more significant compared to the D + V group ($p < 0.05$; Figure 1E). While all groups showed an increase in arterial diastolic blood pressure (DBP) after stimulation, no statistically significant differences were found between them ($p > 0.05$; Figure 1F).

SD induces anxiety- and depression-like behavior in mice

Open-field test (OFT) and elevated plus maze (EPM) tests were conducted (Figures 2A and 2D) to evaluate whether anxiety-like behaviors can be induced in mice by different stimuli. In all stimulus groups, there was a significant decrease in the total running distance compared to that of the control group ($p < 0.001$), as indicated by the results from the OFT. Notably, the most significant reduction in running distance was experienced by the Coriolis illusion group compared to the other stimulus groups ($p < 0.05$; Figure 2B). The percentage of time spent in the central area of the open field was also measured. The results showed a decrease in percentage in all stimulus groups compared to the control group ($p < 0.001$; Figure 2C). More importantly, the Coriolis illusion group had a more significant reduction in the percentage of time spent in the central area than the other stimulus groups. Still, no significant difference was found between the Coriolis illusion and the single-axis vision-ignoring groups. In the EPM, a significant decrease in the time spent in the open arms ($p < 0.001$) was demonstrated by all stimulus groups compared to the control group. Critically, a more significant decrease in the percentage of time spent in open arms, when compared to the other stimulus groups, ($p < 0.01$) was exhibited by the Coriolis illusion group (Figure 2E). Although there is a similar trend in the difference between the total number of entries into the open arms and the time spent in the open arms among mice groups, the difference was not statistically significant (Figure 2F). These results suggest that both uniaxial and biaxial SD can elicit anxiety-like behavior in mice. In addition, the Coriolis illusion stimulus can induce more severe anxiety-like behaviors in mice.

We also investigated whether different stimuli can induce depressive-like behaviors in mice using the forced swimming test (FST) (Figure 2G). The results demonstrated significantly increased immobility time in all stimulus groups compared to the control group ($p < 0.01$). The Coriolis illusion group showed a more significant increase in immobility time than the other stimulus groups ($p < 0.05$; Figure 2H). These findings suggest that various types of SD stimuli can lead to depressive-like behaviors in mice, with more severe depressive-like behaviors induced by the Coriolis illusion stimulus.

SD impairs the cognitive ability of mice

The spatial memory of mice was assessed using the NOR. The mice were trained for 5 min, exposed to different stimuli, and then allowed 10 min of rest before undergoing the recognition test again in a stationary state (Figure 3A). All stimulus groups had a significantly decreased RI ($p < 0.01$) compared to the control group (Figure 3B). The Coriolis illusion group showed a more substantial decrease in the RI score than the other stimulus groups ($p < 0.05$; Figure 3B). Additionally, the non-spatial memory of mice was measured using the step-down type passive avoidance test (SDT) following a similar training, stimulus, and testing procedure (Figure 3C). The Coriolis illusion group exhibited more errors

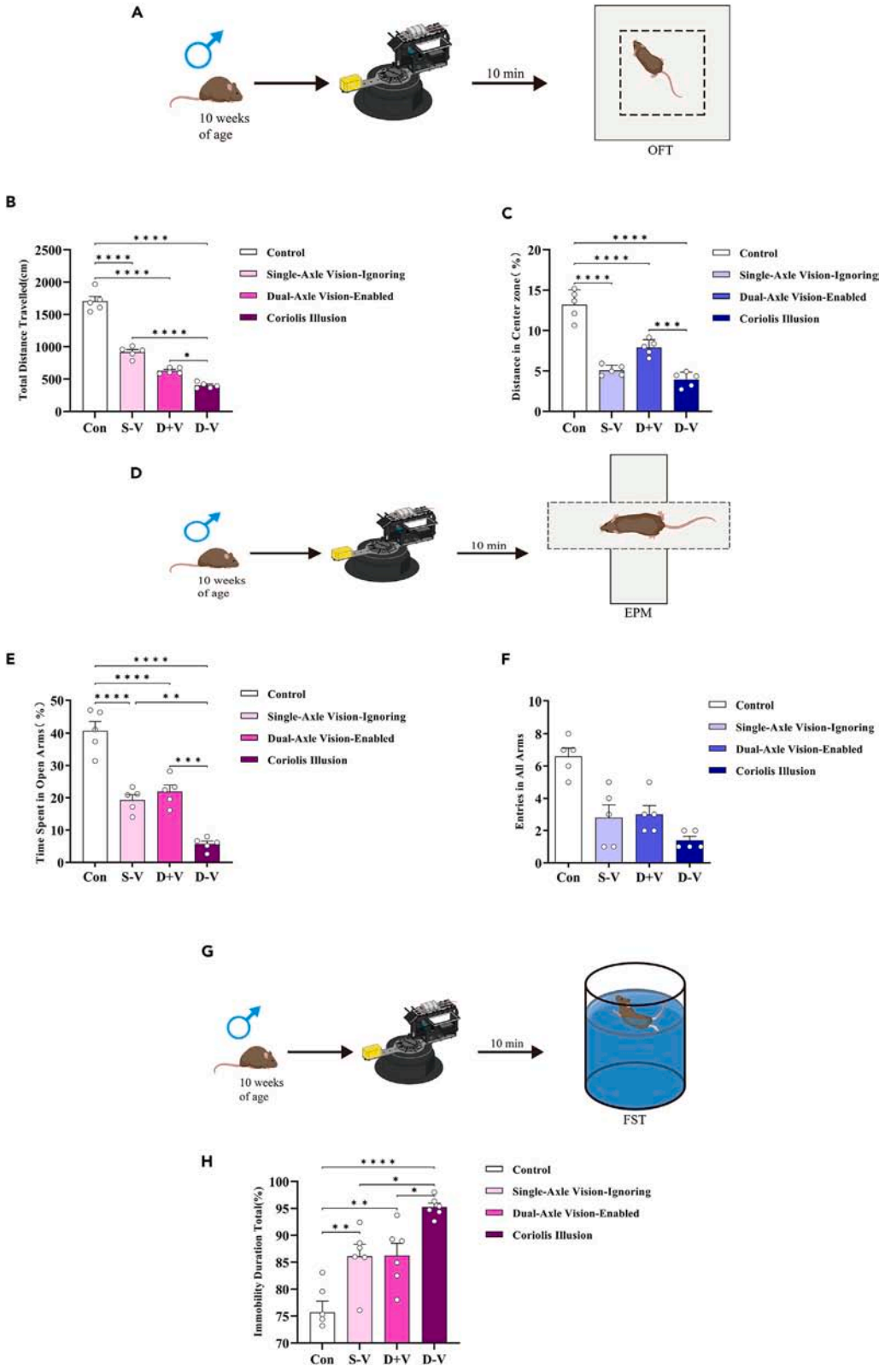
A
10 weeks
of age
10 min
OFT
B
Total Distance Travelled(cm)
Control
Single-Axle Vision-Ignoring
Dual-Axle Vision-Enabled
Coriolis Illusion
Con
S-V
D+V
D-V
C
Distance in Center zone(%)
D
10 min
EPM
E
Time Spent in Open Arms(%)
F
Entries in All Arms
G
10 min
FST
H
Immobility Duration Total(%)

Figure 2. Spatial disorientation induces anxiety and depressive-like behaviors in mice

(A) Experimental procedure.

(B and C) The total distance of activity in the OFT and the proportion of activity in the center area significantly decreased in all rotational groups. The reduction was more significant in the Coriolis illusion group.

(D) Experimental procedure.

(E) The proportion of open-arm activity in each rotation group was significantly reduced, with the Coriolis illusion group showing a more significant reduction.

(F) The groups showed no significant difference in the number of entries into all arms.

(G) Experimental procedure.

(H) The immobility time increased in all rotational groups, with the Coriolis illusion group showing the most significant increase (n = 5 mice per group). Error bars represent ±standard error of the mean. *p < 0.05, **p < 0.01, ***p < 0.001, ****p < 0.0001. OFT, open-field test; EPM, elevated plus maze; FST, forced swimming test.

and higher latency than the other groups (Figures 3D and 3E). These results suggest that various SD stimuli can affect the spatial memory of mice, and severe SD affects both spatial and non-spatial memory.

SD activates neurons in brain regions linked to spatial orientation and memory

After stimulation, several groups of mice were euthanized to obtain sliced brain tissue. Immunofluorescence staining (Figure 4A) showed that both the dentate gyrus (DG) and stratum lucidum (Slu) regions of the hippocampus were activated during both single- and double-axis rotations. (Figures 4B–4D). The fluorescence intensity results of c-Fos in the hippocampal region reveal a significant increase in c-Fos expression in the Coriolis illusion group compared to the other groups ($p < 0.05$). This indicates a prominent activation of hippocampal neurons in the mice of the Coriolis illusion group. (Figure 4E).

SD induced differential expression of messenger RNA in the murine hippocampus

Transcriptomic sequencing was employed to identify mRNA expression levels in different groups of murine hippocampal tissues. A comparison between the Coriolis illusion group and the blank control group revealed a total of 199 aberrantly expressed mRNAs, with 78 mRNAs upregulated (39%) and 121 mRNAs downregulated (61%; Figure 5A). When comparing the Coriolis illusion group to the S-V group, a total of 150 mRNA expression abnormalities were observed, with 71 mRNAs upregulated (47%) and 79 mRNAs downregulated (53%; Figure 5B). In the comparison between the Coriolis illusion group and the D + V group, a total of 300 mRNA expression abnormalities were found, with 64 mRNAs upregulated (21%) and 236 mRNAs downregulated (79%; Figure 5C). Using UpSet Venn analysis to identify genes with differentially expressed patterns exclusively in the Coriolis illusion group compared to the remaining groups, three mRNAs were consistently found to be downregulated in the illusion group compared to the other groups (Figure 5D). These mRNAs are solute carrier family 17 member 6 (Slc17a6), gastrulation brain homeobox 2 (Gbx2), and immunoglobulin heavy constant alpha (Igha).

Occurrence of SD maybe associated with the Slc17a6

Using a clustered heatmap, we presented the expression differences of the three identified DEGs among various groups based on UpSet Venn analysis (Figure 6A). These genes exhibit distinct expression patterns across different stimulus groups. Further gene ontology (GO) database analysis revealed the molecular functions associated with the three selected mRNA transcripts (Figure 6B). Slc17a6 was found to be specifically related to neurotransmitter transport, particularly L-glutamate transmembrane transport. Gbx2 was associated with various cellular and tissue development processes, while Igha was involved in immune functions. Considering the impact of SD on cognitive functions within the nervous system, we targeted Slc17a6 for validation. Consistent with the transcriptomic sequencing results, the qRT-PCR analysis showed a significant decrease in the expression of Slc17a6 in the Coriolis illusion group compared to the other groups ($p < 0.01$; Figure 6C).

DISCUSSION

SD is a major contributing factor to fatal aviation accidents and poses a significant risk to flight safety.[3,4] Pilots who experience SD cannot accurately perceive their aircraft's position, movement, or posture concerning the external coordinate system of the ground and the vertical line of gravity.[2] Therefore, research into the underlying mechanisms of SD is essential for developing effective prevention strategies.

The progress in understanding the mechanisms underlying SD has been excruciatingly slow over the years, even in the context of human subjects. Apart from self-reported reactions,[17] there are no apparent indications of vestibular-induced SD. Moreover, the research on animal models in this field has been severely deficient and lagging. Compared to previous studies,[18,19] we have put forward an innovative approach to construct an animal model of vestibular-induced SD through rotational stimuli combined with the blockade of visual information. This approach is based on prior research[12] and can potentially lead to advancements in the study of the mechanisms of SD.

After exposure to SD, individuals frequently exhibit negative emotions like fear, anxiety, and depression.[20,21] The Coriolis illusion, a vestibular illusion, can have a profound psychological impact, often resulting in feelings of fear. Studies have shown that animals experiencing fearful responses often display decreased body temperature, which could be attributed to terminal vasoconstriction.[22] Therefore, we conducted experiments to measure the rectal temperature changes in mice before and after stimulation. A significant difference was observed between the three rotating mice and the control group regarding rectal temperature decrease, with the most pronounced colonic temperature

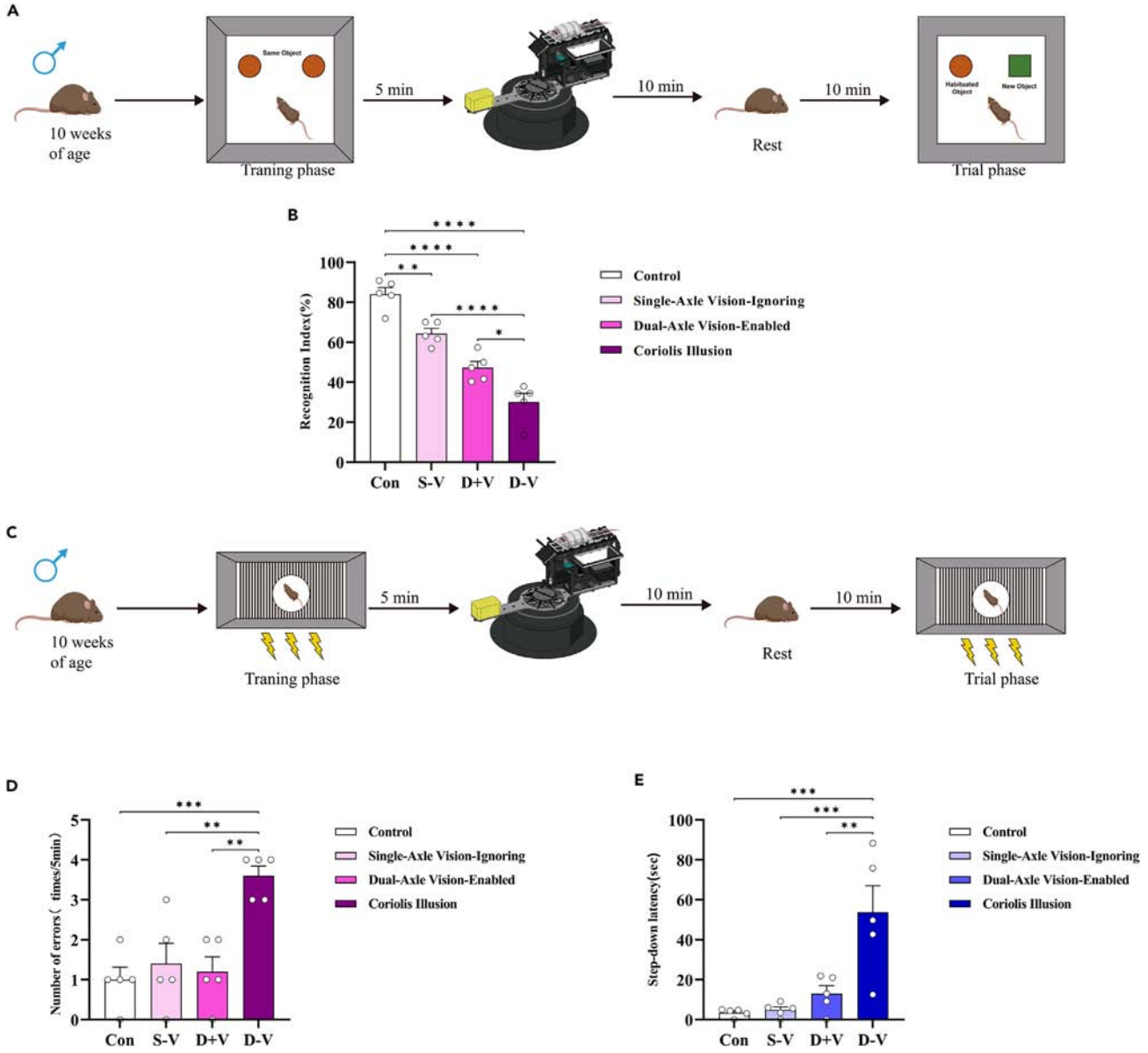

Figure 3. Spatial disorientation impairs cognitive and memory abilities in mice

(A) Experimental procedure.

(B) The RI of all rotation groups decreased significantly compared with the control group, while the Coriolis illusion group showed a significant decrease compared with the other rotation groups.

(C) Experimental procedure.

(D and E) The number of errors and latency period in the Coriolis illusion group significantly increased compared to the other groups (n = 5 mice per group). Error bars represent ±SEM. *p < 0.05, **p < 0.01, ***p < 0.001, ****p < 0.0001. RI, Recognition Index.

decrease observed in the D-V group, which was subjected to visual deprivation. Literature reports suggest that biaxial coupled rotational motion stimulus can cause motion sickness and decrease the animal's body temperature.[23,24] The decrease in rectal temperature in every rotation group may be related to vestibular system stimulation.

In contrast to the D + V group experiencing identical stimulation, the D-V group exhibited a more significant decrease in rectal temperature, likely more closely related to emotional reactions induced by the Coriolis illusion caused by blocking vision. The same rationale can explain why the control group experienced a decrease in rectal temperature, as blocking visual stimuli and immobilizing the mice in a restrainer induced fear responses. In addition, the difference between the D-V group and the D + V group indicates that visual information is crucial for the formation of accurate spatial orientation.[25]

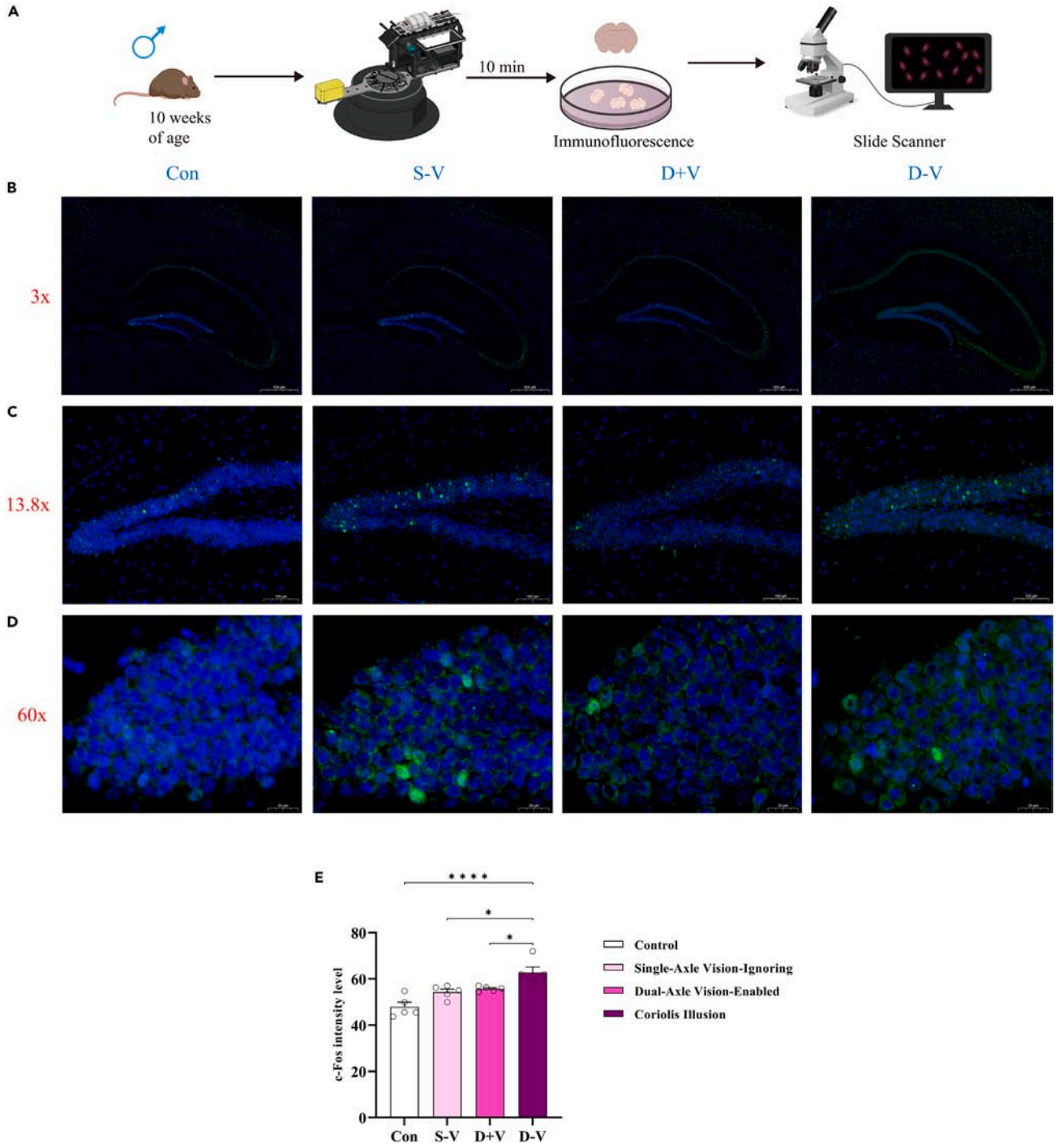

Figure 4. Immunofluorescence staining of a mouse brain section after stimulation

(A) Experimental procedure.

(B) The image from left to right displays the immunofluorescence staining results of the hippocampal-activated neurons in mice exposed to various stimuli across different groups, as observed under a 3-fold magnification.

(C) As observed under a 13.8-fold magnification.

(D) As observed under a 60-fold magnification.

(E) c-Fos intensities in the hippocampus in mice exposed to various stimuli across different groups. The data are presented as individual data points, representing the average of three consecutive fields under a 60-fold magnification (n = 5 mice per group). Error bars represent ±standard error of the mean. *$p < 0.05$, ****$p < 0.0001$.

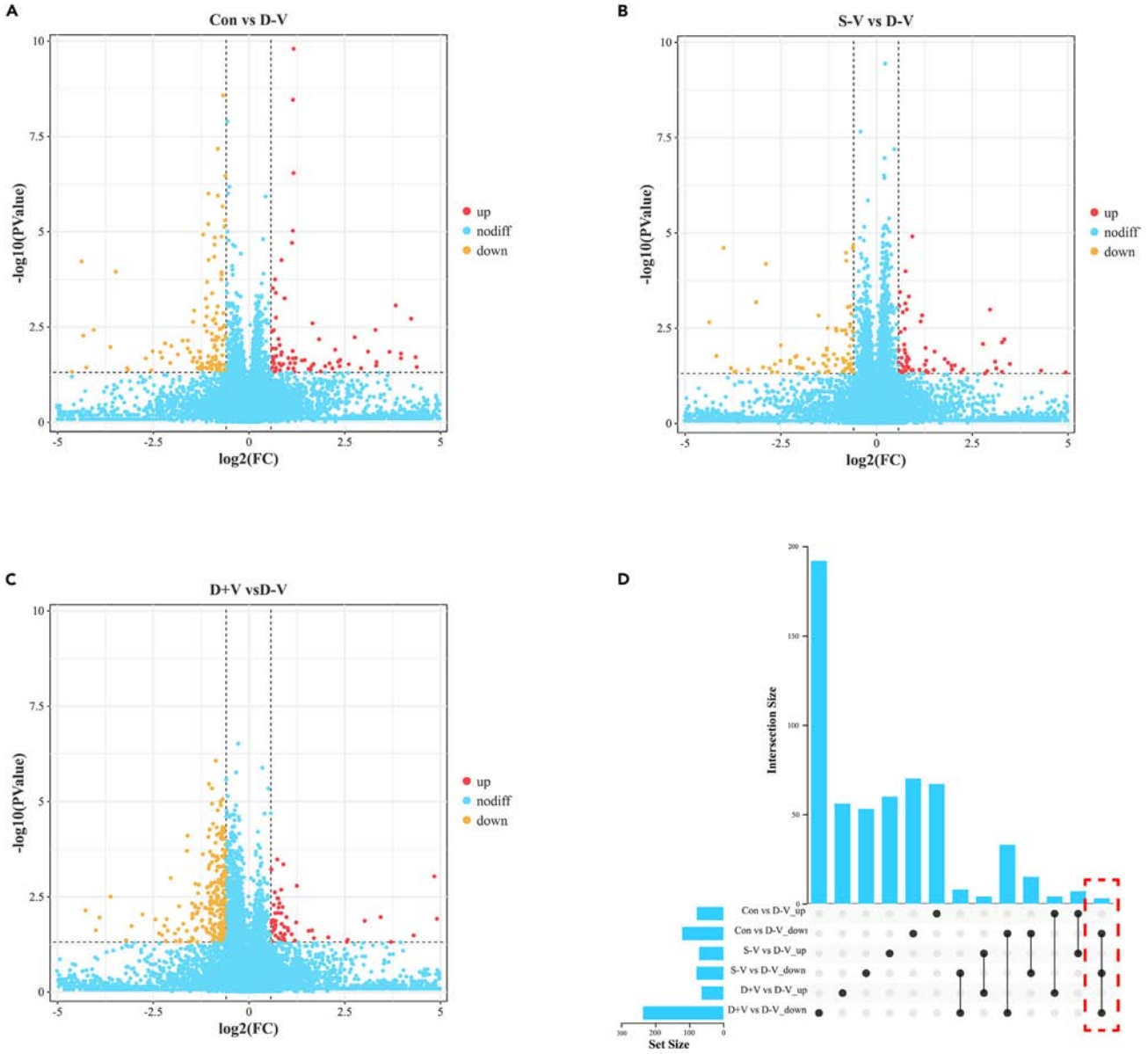

Figure 5. The variation in mRNA expression in the hippocampus of different groups of mice

(A) The volcano plot shows the differential gene expression between the Con group and the D-V group.

(B) The volcano plot shows the differential gene expression between the S-V group and the D-V group.

(C) The volcano plot shows the differential gene expression between the Con, D + V, and the D-V groups.

(D) The UpSet Venn diagram showcases the differential mRNA expression between the D-V group and the remaining groups. The red boxes indicate that all three genes exhibit downregulation in the D-V group when compared to the other groups (n = 5 mice per stimulus group, n = 3 mice in the blank control group). Con, control group; S-V, Single-Axle Vision-Ignoring group; D + V, Dual-Axle Vision-Enabled group; D-V, Coriolis Illusion group.

We observed changes in the blood pressure of mice after experiencing various types of SD. Studies conducted on humans have shown that vestibular rotation stimulation causes an increase in arterial diastolic pressure, while there is no significant change in systolic pressure.[26] However, the results of our measurements of groups of mice before and after stimulation differed from the previous findings. This discrepancy may be attributed to two reasons. First, vestibular rotation stimulation without blocking the visual information is not equivalent to the Coriolis illusion. Second, since we measured the arterial blood pressure in an awake state using indirect measuring equipment, the diastolic pressure values obtained may not be accurate.[27–29] Based on the changes in two physiological parameters, namely rectal temperature and blood pressure, rodents exhibit sympathetic nervous system excitation following SD. This indicates a decrease in blood supply to the peripheral vessels, which causes blood to flow back to the larger vessels. This, in turn, leads to a reduction in rectal temperature and an increase in blood pressure.

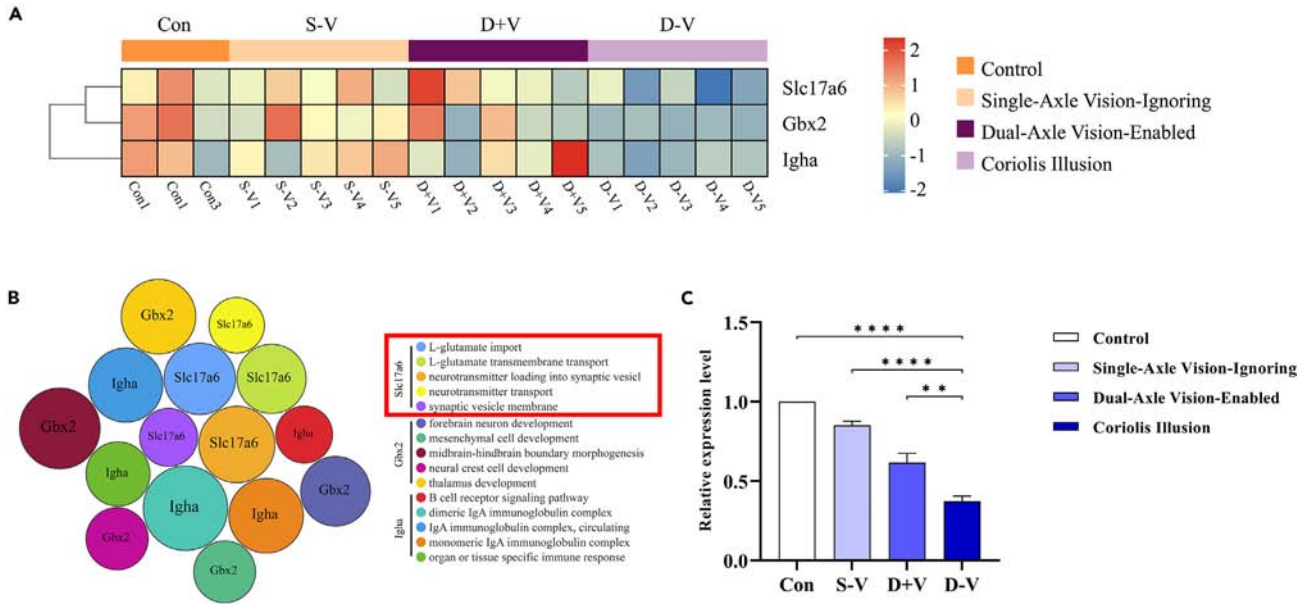

Figure 6. The target gene was identified through screening, and its relative expression level was subsequently validated

(A) The heatmaps depict the expression levels of the three downregulated genes throughout the transcriptome sequencing samples. Red indicates high gene expression levels, while blue indicates low gene expression levels.

(B) The gene ontology (GO) enrichment bubble plot for the three downregulated genes. The GO functions associated with the target gene are highlighted within the red box.

(C) The relative expression levels of the target gene Slc17a6 across different groups (n = 3 mice per group). Error bars represent ±standard error of the mean. **p < 0.01, ****p < 0.0001.

Behavior science experiments are divided into emotion-related and cognition/memory-related. In emotion-related experiments, analysis of the OFT results indicates that various types of SD trigger anxious and depressive symptoms in mice,[30–32] with the Coriolis illusion group demonstrating more pronounced symptoms. The results of the EPM were consistent[33] with those of the OFT, except the total number of arm entries, which did not show any statistically significant difference. This could be attributed to the mice experiencing reduced activity levels following SD stimulation, which was observed by the total distance traveled during the OFT. It is possible that all four stimulus types induced stress in mice,[34,35] causing them to remain in the central area of the EPM after entering and exhibiting limited movement overall.

Consequently, this resulted in a statistical divergence in the proportion of time spent in the open arms but not in the total number of arm entries. Considering the aspects mentioned earlier, we conducted the FST[36] involving physical activity to reduce the incidence of false positive findings for anxiety and depression in mice who typically exhibit reluctance to exercise due to stress. The FST yielded results that align with those obtained through the OFT and EPM, indicating that SD leads to anxious and depressive symptoms in mice,[37] with the Coriolis illusion stimulus type inducing the most prominent symptoms.

Because of the high stimulation level in the SDT,[38] NOR[39] was carried out first. The results indicated that mice experiencing SD exhibited a reduced spatial cognitive ability,[40,41] with the most significant decrease observed in the group of mice experiencing the Coriolis illusion. In the SDT, memory ability[42] was only decreased in mice in the Coriolis illusion group. However, it is important to note that the latency period, representing the time taken for the first jump off the platform, in this group of mice was the greatest, which could have caused hesitation among the mice to move onto the plastic platform because of the stress they experienced.

Therefore, in this study, we employed a unique experimental configuration to induce two types of vestibular SD in mice using different rotating stimuli. One of these types of SD, the Coriolis illusion, results from a more robust and complex stimulation and significantly impacts various physiological and psychological aspects. The Coriolis illusion has a more pronounced impact on mice than other types of SD. It leads to significant decreases in rectal temperature and increased systolic blood pressure. Additionally, it induces severe anxiety and depressive symptoms in mice, impacting their spatial cognition and memory.

The hippocampus plays a vital role in spatial cognition because it is one of the core brain areas involved in spatial navigation and memory formation. The place cells in the hippocampus establish a cognitive map[43] to guide movements in the current environment and have a memory function for the cognitive map. In the final phases of the study, we examined neuron activation in these brain regions in different groups of mice using immunofluorescence staining. We observed neuronal activation in the DG and Slu regions of the hippocampus in all experimental groups, excluding the control group. Furthermore, the statistical analysis of c-Fos fluorescence intensity, representing the degree of neuronal activation, revealed a significant increase in hippocampal neuronal activation in the mice exposed to the Coriolis illusion compared to those in

other groups. This finding provides additional evidence for the robustness of our model construction and evaluation method, as it aligns with the observed neural alterations in nuclei clusters associated with spatial orientation.

Furthermore, immunofluorescence staining results suggest that the mechanism underlying SD, particularly for complex disorientation, could be associated with activating neurons in the hippocampus. Subsequently, we performed transcriptome sequencing on the hippocampal tissue of mice from different groups and employed bioinformatics methods such as UpSet Venn analysis and GO enrichment analysis to analyze differentially expressed mRNAs between the Coriolis illusion group and the other groups. The objective was to explore potential molecular mechanisms underlying the observed discrepancies. Among the three identified genes with abnormal expression, Slc17a6 has been extensively reported in previous literature to be closely associated with alterations in cognitive function.[44,45] Considering the correlation between SD formation and cognitive functional changes, we selected Slc17a6 as the target gene and utilized qRT-PCR to validate the observed abnormal mRNA expression. The results unequivocally demonstrated the aberrant expression of Slc17a6 in the SD model.

Slc17a6 serves as the gene encoding the vesicular glutamate transporter 2 (VGlut2),[46] a protein that facilitates the selective loading of glutamate into synaptic vesicles and promotes its release. Glutamate is a primary excitatory neurotransmitter in the central nervous system,[47] playing a crucial role in regulating synaptic transmission within the central nervous system. It modulates various functions in the normal brain, such as learning, memory, movement, and cognition. The downregulation of Slc17a6 can disrupt glutamate signaling in the hippocampus, leading to reduced synaptic activity and impaired cognitive function in mice.[46] Further, it may also contribute to decreased cell count and structural disorganization.[48] Intriguingly, the activation of neurons in the hippocampal region appears to be inversely related to the expression of Slc17a6. We speculate that the neurons activated in this region may be inhibitory neurons. However, further experiments should be conducted to investigate the specific mechanisms involved in this phenomenon.

Limitations of the study

An ideal animal model should possess objective evaluation parameters, particularly indicators that can measure changes throughout the entire process. However, spatial disorientation is a transient and functional impairment rather than an organic alteration. Perusing various pertinent literatures, it becomes evident that even in cases where the subjects are sentient humans capable of autonomous subjective articulation, there is a dearth of real-time objective methods to appraise spatial orientation aptitude. Most commonly employed approaches involve subjective reports from participants regarding their experiences, along with the assessment of various objective indicators before and after the occurrence of spatial orientation impairments.[17,20,49,50] Our assessment methods for mice are based on observed physiological and psychological changes in human subjects with spatial orientation impairments. However, in our quest to explore real-time of assessment, the essential prerequisite for mice to sustain a perpetual state of wakefulness devoid of anesthesia throughout the entirety of the experiment renders the utilization of invasive techniques for real-time monitoring unfeasible. Additionally, the wireless telemetry sensors demonstrate unreliability in collecting pertinent data during rapid rotation. Similarly, we may encounter limitations in utilizing electrophysiology and wireless electroencephalogram (EEG) monitoring techniques to achieve real-time assessment of neurologic changes. In future experiments, our aim is to improve the rotational device employed to stimulate the mice, minimizing the production of excessive vibrations. Simultaneously, once the stability of the wireless telemetry devices has been enhanced, we will incorporate them to facilitate the real-time assessment of physiological parameters. This enhancement will enable us to gather a wealth of valuable data during the experiments. Moreover, the establishment of this animal model itself serves the purpose of seeking additional objective indicators concerning the occurrence of spatial disorientation through an in-depth exploration of its underlying mechanisms. Furthermore, we will conduct further investigations into the molecular mechanisms underlying Slc17a6, aiming to elucidate the microscale mechanisms involved in the occurrence of SD with utmost clarity.

Conclusions

In this study, we proposed a method for the construction and evaluation of a mouse model of vestibular SD. Specifically, we developed the model by stimulating the semicircular canals with a double-axis coupled rotation device while blocking vision. We assessed the model by monitoring multiple physiological parameters in mice after exposure to SD and investigating its psychological effects, particularly its impact on cognition and memory. Thereafter, we delved into the neuronal alterations within brain regions associated with normal spatial orientation, thereby establishing the presence of excessive activation in the hippocampal region during the onset of SD. Subsequently, we employed transcriptomic sequencing and bioinformatics techniques to elucidate the potential involvement of Slc17a6 in SD and confirmed the downregulation of Slc17a6 in the hippocampus of the SD model mice through qRT-PCR technology. These findings provide further substantiation for the viability of our approach in model development and evaluation while laying the groundwork for further exploration of its underlying molecular mechanisms in greater depth.

STAR★METHODS

Detailed methods are provided in the online version of this paper and include the following:

- KEY RESOURCES TABLE
- RESOURCE AVAILABILITY
  - Lead contact
  - Materials availability
  - Data and code availability

SUPPLEMENTAL INFORMATION

Supplemental information can be found online at https://doi.org/10.1016/j.isci.2023.108498.

ACKNOWLEDGMENTS

We are grateful for the sequencing platform and bioinformation analysis of Gene Denovo Biotechnology Co., Ltd (Guangzhou, China).

Supported by Air Force Medical University Special Program for Guiding First-rate Aerospace Medicine Disciplines and Supporting Excellent Doctoral and Master's Students (2022YSZC04).

AUTHOR CONTRIBUTIONS

C.T., W.X.C., and L.Y. conceived and designed the experiment methods. C.T., Z.M., Z.J., and W.H. organized experiments and constructed mouse model. C.T., Z.M., W.K., and W.H.T. evaluated the model. C.T. and Z.Z.R. subjected hippocampal tissue to sampling and performed qRT-PCR experiments. C.T., Z.J., W.F., and Z.Z.R. conducted the statistics. C.T., L.C.C., and Y.J.H. drafted the manuscript. Z.M., W.X.C., and L.Y. revised the manuscript. W.X.C. and L.Y. helped perform the analysis with constructive discussions. All authors take responsibility for the integrity of the data and the accuracy of data analysis.

DECLARATION OF INTERESTS

The authors declare no competing interests.

INCLUSION AND DIVERSITY

We support inclusive, diverse, and equitable conduct of research.

Received: July 1, 2023
Revised: October 8, 2023
Accepted: November 17, 2023
Published: November 21, 2023

REFERENCES

1. Lessard, C.S. (2000). Spatial disorientation: dealing with aeronautical illusions. IEEE Eng. Med. Biol. Mag. *19*, 25–27.
2. Meeks, R.K., Anderson, J., and Bell, P.M. (2023). Physiology of Spatial Orientation.
3. Gibb, R., Ercoline, B., and Scharff, L. (2011). Spatial disorientation: Decades of pilot fatalities. Aviat Space Environ. Med. *82*, 717–724.
4. Newman, R.L., and Rupert, A.H. (2020). The Magnitude of the Spatial Disorientation Problem in Transport Airplanes. Aerosp. Med. Hum. Perform. *91*, 65–70.
5. Pennings, H.J.M., Oprins, E.A.P.B., Wittenberg, H., Houben, M.M.J., and Groen, E.L. (2020). Spatial Disorientation Survey Among Military Pilots. Aerosp. Med. Hum. Perform. *91*, 4–10.
6. Cheung, B. (2013). Spatial disorientation: more than just illusion. Aviat Space Environ. Med. *84*, 1211–1214.
7. Hao, C., Fan, X., Dong, C., Qiao, L., Li, X., Li, X., Cheng, L., Guo, L., and Zhao, R. (2020). A Classification Method for Unrecognized Spatial Disorientation Based on Perceptual Process. IEEE Access *8*, 140654–140660.
8. Semenov, L.V., and Bures, J. (1989). Vestibular stimulation disrupts acquisition of place navigation in the Morris water tank task. Behav. Neural. Biol. *51*, 346–363.
9. Martin, G.M., Harley, C.W., Smith, A.R., Hoyles, E.S., and Hynes, C.A. (1997). Spatial disorientation blocks reliable goal location on a plus maze but does not prevent goal location in the Morris maze. J. Exp. Psychol. Anim. Behav. Process. *23*, 183–193.
10. Calton, J.L., and Taube, J.S. (2005). Degradation of head direction cell activity during inverted locomotion. J. Neurosci. *25*, 2420–2428.
11. Valerio, S., Clark, B.J., Chan, J.H.M., Frost, C.P., Harris, M.J., and Taube, J.S. (2010). Directional learning, but no spatial mapping by rats performing a navigational task in an

inverted orientation. Neurobiol. Learn. Mem. *93*, 495–505.
12. Grieves, R.M., Shinder, M.E., Rosow, L.K., Kenna, M.S., and Taube, J.S. (2022). The Neural Correlates of Spatial Disorientation in Head Direction Cells. eNeuro *9*. ENEURO.0174, 22.2022.
13. Stackman, R.W., Clark, A.S., and Taube, J.S. (2002). Hippocampal spatial representations require vestibular input. Hippocampus *12*, 291–303.
14. Paillard, A.C., Quarck, G., and Denise, P. (2014). Sensorial countermeasures for vestibular spatial disorientation. Aviat Space Environ. Med. *85*, 563–567.
15. Sánchez-Tena, M.Á., Alvarez-Peregrina, C., Valbuena-Iglesias, M.C., and Palomera, P.R. (2018). Optical Illusions and Spatial Disorientation in Aviation Pilots. J. Med. Syst. *42*, 79.
16. Pancratz, D.J., Bomar, J.B., Jr., Raddin, J.H., Jr., and Raddin, J.H. (1994). A new source for vestibular illusions in high agility aircraft. Aviat Space Environ. Med. *65*, 1130–1133.
17. Kang, Y., Lazaro, M.J., and Kim, S. (2021). Crosschecking through verbal reports under spatial disorientation scenarios: Evidence from eye tracking metrics. Int. J. Ind. Ergon. *86*, 103202.
18. Wang, R.F., and Spelke, E.S. (2000). Updating egocentric representations in human navigation. Cognition *77*, 215–250.
19. Sargent, J., Dopkins, S., Philbeck, J., and Modarres, R. (2008). Spatial memory during progressive disorientation. J. Exp. Psychol. Learn. Mem. Cogn. *34*, 602–615.
20. Tornero Aguilera, J.F., Gil-Cabrera, J., and Clemente-Suárez, V.J. (2022). Determining the psychophysiological responses of military aircrew when exposed to acute disorientation stimuli. BMJ Mil. Health *168*, 112–116.
21. Kang, Y., Yun, M.H., and Kim, S. (2020). Verbal Reports Influence on Pilot Flight Performance and Mental Stress Under Spatial Disorientation. Aerosp. Med. Hum. Perform. *91*, 948–955.
22. Vianna, D.M.L., and Carrive, P. (2005). Changes in cutaneous and body temperature during and after conditioned fear to context in the rat. Eur. J. Neurosci. *21*, 2505–2512.
23. Tu, L., Poppi, L., Rudd, J., Cresswell, E.T., Smith, D.W., Brichta, A., and Nalivaiko, E. (2017). Alpha-9 nicotinic acetylcholine receptors mediate hypothermic responses elicited by provocative motion in mice. Physiol. Behav. *174*, 114–119.
24. Nobel, G., Tribukait, A., Mekjavic, I.B., and Eiken, O. (2012). Effects of motion sickness on thermoregulatory responses in a thermoneutral air environment. Eur. J. Appl. Physiol. *112*, 1717–1723.
25. Zheng, Q., Zhou, L., and Gu, Y. (2021). Temporal synchrony effects of optic flow and vestibular inputs on multisensory heading perception. Cell Rep. *37*, 109999.
26. Li, S., Zhang, Y., and Sun, X. (2022). Effects of vestibular stimulation on cardiovascular function and cognitive ability. Chin Heart J. *34*, 455–460.
27. Drüeke, T.B., and Devuyst, O. (2019). Blood pressure measurement in mice: tail-cuff or telemetry. Kidney Int. *96*, 36.
28. Wang, Y., Thatcher, S.E., and Cassis, L.A. (2017). Measuring Blood Pressure Using a Noninvasive Tail Cuff Method in Mice. Methods Mol. Biol. *1614*, 69–73.
29. Feng, M., and DiPetrillo, K. (2009). Non-invasive blood pressure measurement in mice. Methods Mol. Biol. *573*, 45–55.
30. Zeldetz, V., Natanel, D., Boyko, M., Zlotnik, A., Shiyntum, H.N., Grinshpun, J., Frank, D., Kuts, R., Brotfain, E., and Peiser, J. (2018). A New Method for Inducing a Depression-Like Behavior in Rats. J. Vis. Exp. *10*, 57137.
31. Song, A.Q., Gao, B., Fan, J.J., Zhu, Y.J., Zhou, J., Wang, Y.L., Xu, L.Z., and Wu, W.N. (2020). NLRP1 inflammasome contributes to chronic stress-induced depressive-like behaviors in mice. J. Neuroinflammation *17*, 178.
32. Hu, C., Luo, Y., Wang, H., Kuang, S., Liang, G., Yang, Y., Mai, S., and Yang, J. (2017). Re-evaluation of the interrelationships among the behavioral tests in rats exposed to chronic unpredictable mild stress. PLoS One *12*, e0185129.
33. Seibenhener, M.L., and Wooten, M.C. (2015). Use of the Open Field Maze to measure locomotor and anxiety-like behavior in mice. J. Vis. Exp. e52434.
34. Komada, M., Takao, K., and Miyakawa, T. (2008). Elevated plus maze for mice. J. Vis. Exp. 1088.
35. Carola, V., D'Olimpio, F., Brunamonti, E., Mangia, F., and Renzi, P. (2002). Evaluation of the elevated plus-maze and open-field tests for the assessment of anxiety-related behaviour in inbred mice. Behav. Brain Res. *134*, 49–57.
36. Unal, G., and Canbeyli, R. (2019). Psychomotor retardation in depression: A critical measure of the forced swim test. Behav. Brain Res. *372*, 112047.
37. Kraeuter, A.K., Guest, P.C., and Sarnyai, Z. (2019). The Elevated Plus Maze Test for Measuring Anxiety-Like Behavior in Rodents. Methods Mol. Biol. *1916*, 69–74.
38. Kameyama, T., Nabeshima, T., and Kozawa, T. (1986). Step-down-type passive avoidance-and escape-learning method. Suitability for experimental amnesia models. J. Pharmacol. Methods *16*, 39–52.
39. Mathiasen, J.R., and DiCamillo, A. (2010). Novel object recognition in the rat: a facile assay for cognitive function. Curr. Protoc. Pharmacol.. Chapter 5, Unit 5.59.
40. Cohen, S.J., and Stackman, R.W., Jr. (2015). Assessing rodent hippocampal involvement in the novel object recognition task. Behav. Brain Res. *285*, 105–117.
41. Antunes, M., and Biala, G. (2012). The novel object recognition memory: neurobiology, test procedure, and its modifications. Cognit. Process. *13*, 93–110.
42. Hiramatsu, M., and Inoue, K. (1999). Nociceptin/orphanin FQ and nocistatin on learning and memory impairment induced by scopolamine in mice. Br. J. Pharmacol. *127*, 655–660.
43. Buzsáki, G., and Moser, E.I. (2013). Memory, navigation and theta rhythm in the hippocampal-entorhinal system. Nat. Neurosci. *16*, 130–138.
44. Zhang, C.R., Ho, M.F., Vega, M.C.S., Burne, T.H.J., and Chong, S. (2015). Prenatal ethanol exposure alters adult hippocampal VGLUT2 expression with concomitant changes in promoter DNA methylation, H3K4 trimethylation and miR-467b-5p levels. Epigenet. Chromatin *8*, 40.
45. Wang, Y., Khandelwal, N., Liu, S., Zhou, M., Bao, L., Wang, J.E., Kumar, A., Xing, C., Gibson, J.R., and Wang, Y. (2022). KDM6B cooperates with Tau and regulates synaptic plasticity and cognition via inducing VGLUT1/2. Mol. Psychiatr. *27*, 5213–5226.
46. Melief, E.J., McKinley, J.W., Lam, J.Y., Whiteley, N.M., Gibson, A.W., Neumaier, J.F., Henschen, C.W., Palmiter, R.D., Bamford, N.S., and Darvas, M. (2018). Loss of glutamate signaling from the thalamus to dorsal striatum impairs motor function and slows the execution of learned behaviors. NPJ Parkinsons Dis. *4*, 23.
47. Kashani, A., Betancur, C., Giros, B., Hirsch, E., and El Mestikawy, S. (2007). Altered expression of vesicular glutamate transporters VGLUT1 and VGLUT2 in Parkinson disease. Neurobiol. Aging *28*, 568–578.
48. Schweizer, N., Viereckel, T., Smith-Anttila, C.J., Nordenankar, K., Arvidsson, E., Mahmoudi, S., Zampera, A., Wärner Jonsson, H., Bergquist, J., Lévesque, D., et al. (2016). Reduced Vglut2/Slc17a6 Gene Expression Levels throughout the Mouse Subthalamic Nucleus Cause Cell Loss and Structural Disorganization Followed by Increased Motor Activity and Decreased Sugar Consumption. eNeuro *3*. ENEURO.0264-0216.
49. Lucertini, M., Bianca, E., Marciano, E., and Pettorossi, V.E. (2019). Analysis of the nystagmus evoked by cross-coupled acceleration (Coriolis phenomenon). Acta Otorhinolaryngol. Ital. *39*, 341–346.
50. Hao, C., Cheng, L., Guo, L., Zhao, R., Wu, Y., Li, X., Chi, Z., Zhang, J., Liu, X., Ma, X., et al. (2022). Detection of unrecognized spatial disorientation: A theoretical perspective. Technol. Health Care *30*, 469–480.

STAR★METHODS

KEY RESOURCES TABLE

REAGENT or RESOURCE	SOURCE	IDENTIFIER
Antibodies		
Mouse monoclonal [83B1138] to Fos B	Abcam	ab11959 Cat.No.:1005347
CoraLite488-conjugated Goat Anti-Mouse IgG(H + L)	Proteintech	SA00013-1 Lot.No.:20000792
Chemicals, peptides, and recombinant proteins		
Paraformaldehyde	Biosharp	BL539A Lot.No.:23067175
Phosphate-Buffered Saline	Servicebio	Cat.No.: G0002
Sucrose	BioFroxx	Cat.No.:1245GR500
Optimum cutting temperature compound	SAKURA	4583 Lot.No.:2582-00
Goat Serum	BOSTER	AR00009 Lot.No.:17H18B09
Triton™ X-100	MP Biomedicals	CAS.No.:9002-93-1
2-(4-Amidinophenyl)-6-indolecarbamidine dihydrochloride	Beyotime	C1006 CAS.No.: 28718-90-3
Critical commercial assays		
Trizol reagent kit	Invitrogen	15596018
Agilent 2100 Bioanalyzer	Agilent Technologies	DE54107949
QiaQuick PCR extraction kit	Qiagen	28106
Illumina Novaseq6000	Illumina	A00265
TSINGKE TSP413 RNAprep FastPure kit	Beijing Tsingke Biotechnology Co	Cat.No.: TSP413 Lot.No.:1AL23401
MightyScript First Strand cDNA Synthesis Master Mix	Sangon	B639251-0100 Lot.No.:J228KA8351
LightCycler 480	Roche	N/A
SYBR Green PCR master mix	Yeasen	Cat.No.: 11201ES08 Lot.No.:H6312070
Deposited data		
Raw data	This paper	GEO: GSE243471
Experimental models: Organisms/strains		
Mouse: C57BL6/J	Experimental Animal Center of Air Force Medical University	N/A
Oligonucleotides		
Slc17a6 forward——5′- GTCGGTAAAACAAAGGATTTTGGC -3′	Tsingke Biotechnology Co	This paper
Slc17a6 reverse——5′- GCTTCTTCTCCAGCACCCTGTA -3′	Tsingke Biotechnology Co	This paper
β-actin forward——5′-AACAGTCCGCCTAGAAGCAC-3′	Tsingke Biotechnology Co	This paper
β-actin reverse——5′-CGTTGACATCCGTAAAGACC-3′	Tsingke Biotechnology Co	This paper
Software and algorithms		
SMART 3.0 software	Panlab HARVARD	N/A
Bioinformatic analysis	Gene Denovo Biotechnology Co	http://www.omicsmart.com
GraphPad Prism 9.5	Insightful Science	N/A

(*Continued on next page*)

Continued

REAGENT or RESOURCE	SOURCE	IDENTIFIER
Other		
ALC-ET03 animal digital electronic thermometer	Oricotech	N/A
BP-2010A animal blood pressure monitor	Softlong Biotech	N/A
Animal vestibular stimulation device	This paper	N/A
OFT box	RWD	N/A
Elevated Plus Maze	RWD	N/A
FST cylinder	RWD	N/A
Pannoramic MIDI	3DHISTECH	N/A

RESOURCE AVAILABILITY

Lead contact

Further information and requests for resources and reagents should be directed to and will be fulfilled by the lead contact, Tong Chang (hkhtgkd@163.com).

Materials availability

This study did not generate new unique reagents.

Data and code availability

Raw mRNA-seq data of all samples were uploaded to the Gene Expression Omnibus (GEO) of the National Center for Biotechnology Information (GSE243471).

This paper did not generate any original code.

All other items: any additional information required to reanalyze the data reported in this paper is available from the lead contact upon request.

EXPERIMENTAL MODEL AND STUDY PARTICIPANT DETAILS

Animal groups

We obtained male C57BL/6 mice from the Experimental Animal Center of Air Force Medical University. These mice were 9 weeks of age and weighed 23.7 $\pm$ 1.4 g [mean $\pm$ standard error of the mean (SEM)]. We maintained these animals under controlled conditions of 25°C, 12-h light/12-h dark lighting, and approximately 40–50% humidity, with *ad libitum* access to food and water. We fully complied with the National Regulations for the Management of Laboratory Animals, and the Ethics Committee for Animal Welfare of Air Force Medical University in Xi'an, China, approved the study (license number: SCXK [Shaanxi] 2019-001).

Following a one-week acclimation period to the animal room, we confirmed that the body weight of the mice exceeded 25 g, allowing for their positioning in the self-developed mouse fixation device (Figures S1A and S1B). We then randomly assigned 20 mice into four groups, with 5 mice per group. The first group was the control (Con) group, and the second group underwent unidirectional rotational motion with visual occlusion. It was referred to as the Single-Axle Vision-Ignoring (S-V) group. This group of mice was designed to be a simple SD group based on previous research.[12,18,19] The third group, called the double-axis vision (D + V) group, underwent bidirectional rotational motion without visual occlusion. Since spatial orientation abilities involve the integration of various sensory information in the brain, we designed this group to investigate whether the mice would still exhibit more complex SD (i.e., Coriolis illusion) or reduce the related behaviors after being stimulated by biaxial rotation under the premise of having good visual cue input. Finally, we induced the Coriolis illusion in the fourth group using bidirectional rotational motion with visual occlusion, and this group was referred to as the Coriolis illusion (D-V) group. To better simulate the Coriolis illusion, which often occurs in poor visual conditions in natural flight environments,[15] we deprived the mice in this group of their vision. Following exposure to different stimuli, the groups of mice were subjected to various experiments, which included measurements of physiological parameters, behavioral changes, and additional analyses.

Model construction and procedure

Our self-developed animal vestibular stimulation device generated the SD stimulus during the experiment, enabling separate or combined rotation along the animals' semicircular canals in three different planes. First, the mice were fixed in a self-made restraint, and when visual shielding was required, they were masked with an opaque black cloth to block their vision (Figure S1A); when visual stimulation was needed, the cloth was removed (Figure S1B). The mice were then situated on a specially designed rotating apparatus for various experiments. In the control group, the mice were also restrained within the apparatus while visually occluded and not disturbed for 10 min (Figure S1C). In the S-V

group, the mice were similarly restrained with visual occlusion, but the rotating device was rotated around the vertical axis at a speed of 180°/second for 10 min (Figure S1D). In the D + V group, the hood was removed with the mice still restrained. The device was rotated around both the vertical axis (speed of 180°/s) and the longitudinal axis of the mouse body (rotation angle of 1 cycle: +30°∼-30°, speed of 1.5 s/cycle) for 10 min (Figure S1E). In the D-V group, the mice were restrained with visual occlusion and stimulated like in the D + V group (Figure S1F).

METHOD DETAILS

Rectal temperature and arterial blood pressure measurement in mice

A total of 20 mice were included in this study, and divided into four groups of five mice for measuring physiological parameters. Before and after the stimuli, the rectal temperature of the mice was measured using an ALC-ET03 animal digital electronic thermometer (Oricotech, Shanghai, China). The thermometer probe was inserted approximately 3 cm into the rectum of each mouse. Additionally, the arterial pressure of the mice was indirectly measured using the BP-2010A animal blood pressure monitor (Softlong Biotech, Beijing, China) by applying the device to their tails.

Behavioral analysis

The mice were randomly divided into four groups, each consisting of five mice, for emotion-related behavioral tests. All behavioral tests were conducted during the light cycle. On the day of the test, the mice were transferred to the testing room 2 h before the test began and were subjected to 10 min of different SD stimuli before initiating the behavioral test. All tests were completed between 8:00 a.m. and 3:00 p.m., and there was a 2-day interval between adjacent emotion-related behavioral tests. The more stressful forced swimming test (FST) was performed last to prevent the intense stimulation from affecting the results. After completing the FST, a new batch of mice was used to avoid the effects of strong stimulation. The cognitive and memory-related behavioral tests were conducted with a 2-day interval between adjacent tests, and the more stressful platform jump test was performed last. Before and after each behavioral test, 75% ethanol was sprayed to eliminate odor interference.

Open-field test (OFT)

The mice were tested in an OFT box (40 cm × 40 cm × 40 cm) (RWD, Shenzhen, China). They were placed in the center area of the open field (Figure 1), and each time, the animal was placed in the center of the test box from the same position and direction. The mice were allowed to move freely in the open field for 8 min, and SMART 3.0 software (Panlab HARVARD, MA, USA) was used to determine the total distance traveled by the mice and the percentage of time spent in the center area of the open field.

Elevated plus maze (EPM)

The mice were placed in an EPM (RWD, Shenzhen, China) consisting of two open arms (30 cm × 5 cm × 1 cm), two closed arms (30 cm × 5 cm × 15 cm), and a central area (5 cm × 5 cm), with a height of 50 cm from the ground for testing. At the beginning of the test, the mice were placed in the central area, facing one open arm direction. The mice were allowed to move freely for 8 min, and SMART 3.0 software (Panlab HARVARD, MA, USA) was used to record the total number of entries into the open and closed arms and the percentage of time spent in the open arms and closed arms.

Forced swimming test

The mice were placed in an FST cylinder (RWD, Shenzhen, China) with the following dimensions: a height of 30 cm, a diameter of 12 cm, and a water depth of 15 cm. To ensure that the mice floated freely without any external support, their tails were kept from touching the bottom of the cylindrical container filled with water. The water temperature was controlled at 23°C–25°C, and SMART 3.0 software (Panlab HARVARD, MA, USA) was used to record their behavior within 6 min. The immobility time was calculated for From the second to the sixth minute (total of 5 min). (i.e., when the mouse stopped struggling in the water and floated with only slight limb movements to keep its head above the water). After each mouse was tested, the water was changed to eliminate odor interference.

Novel object recognition (NOR)

Different stimuli were used based on each group according to the experimental design mentioned previously. First, the mice were placed in the open-field arena with two identical cone sand allowed to freely explore the open-field arena for 5 min. Following the cessation of the stimulus, the mice were granted a period of tranquility lasting 10 min, wherein the cone on the right-hand side was replaced by a cube (possessing the same height as the aforementioned cone), thus introducing an unfamiliar object. The mice were then returned to the arena for 5 min of free exploration. We recorded the time the mice interacted (sniffing or exploring the object within 2 cm) with the new and old objects. Using this information, we calculated the recognition index (RI) by dividing the time the mice spent interacting with the new object by the total time the mice spent interacting with both new and old objects, multiplied by 100. Data recording and analysis were conducted using SMART 3.0 software (Panlab HARVARD, MA, USA).

Step-down type passive avoidance test (SDT)

The experimental apparatus comprised a plastic box with an iron wire at the bottom that discharged every 2 s with a current intensity of 10 mA and a plastic avoidance platform. Each mouse was acclimatized to the environment for 5 min at the beginning of each training session. The electric wire was activated during that time, prompting the mouse to jump onto the avoidance platform to avoid the electric shock. Different stimuli were then applied. After stimulation, each mouse was allowed to rest for 10 min before being placed back in the box on the plastic avoidance platform. The time taken for each mouse to jump off the platform for the first time (i.e., the latent period) and the number of errors (i.e., the number of times each mouse jumped off the platform within 5 min) were recorded for analysis. The SDT was conducted as described previously. Data recording and analysis were performed using SMART 3.0 software (Panlab HARVARD, MA, USA).

Fos immunofluorescence

Twenty mice were divided into four groups of five for Fos immunofluorescence analysis, with each group receiving one type of rotational stimulation as previously outlined. After anesthesia with pentobarbital (0.03 mL/10 g), the brains were promptly fixed with 4% paraformaldehyde in phosphate-buffered saline (PBS) (pH 7.4–7.5) at 4°C overnight. Subsequently, the brains were dehydrated in a 30% sucrose solution at 4°C for 72 h, embedded in optimum cutting temperature compound (SAKURA, CA, USA), and frozen at −80°C for 10 min to preserve their structure. Using a vibratome (Leica, CM3050S, Wetzlar, Germany), the brains were sliced coronally into 8 μm sections. After sectioning, the brains were washed three times with PBS (pH 7.4–7.5), blocked with a solution containing 5% goat serum (AR0009, BOSTER, Wuhan, China) and 0.25% Triton X-100 (MP Biomedicals, CA, USA) for 1 h, and incubated with primary antibodies against Fos B (1:500, ab11959, Abcam, Cambs, UK) for 72 h at 4°C. The sections were then incubated with 488-labeled goat anti-Mouse IgG (H + L) (1:200, SA00013-1, Proteintech, IL, USA) at 26°C for 2 h. The nuclei were stained with 2-(4-Amidinophenyl)-6-indolecarbamidine dihydrochloride (DAPI, Beyotime, Shanghai, China), and the brain sections were washed three times with PBS before and after staining. Finally, the brain tissue sections were mounted on a slide and scanned using a slide scanner (Pannoramic MIDI, 3DHISTECH, Budapest, Hungary). All slices were stained simultaneously and imaged at fixed intensity settings, allowing for direct comparison of c-Fos intensities between groups within the hippocampal region, thereby providing information about the degree of c-Fos expression rather than the number of positive cells.

RNA extraction, library construction, and sequencing

Using the abovementioned modeling approach, we subjected 18 mice to stimulation and immediately euthanized them to extract hippocampal tissue. The mice were divided into the following groups: three mice in the blank control group, five mice in the S-V group, five mice in the D + V group, and five mice in the D-V group. According to the manufacturer's protocol, hippocampal total RNA was extracted using a Trizol reagent kit (Invitrogen, Carlsbad, CA, USA). RNA quality was assessed on an Agilent 2100 Bioanalyzer (Agilent Technologies, Palo Alto, CA, USA) and checked using RNase-free agarose gel electrophoresis. After total RNA was extracted, eukaryotic mRNA was enriched by Oligo(dT) beads. Thereafter, the enriched mRNA was fragmented into short fragments using a fragmentation buffer and reverse transcripted into cDNA with random primers. Second-strand cDNA was synthesized by DNA polymerase I, RNase H, dNTP, and buffer. The cDNA fragments were purified with a QiaQuick PCR extraction kit (Qiagen, Venlo, The Netherlands), end-repaired, poly(A) added, and ligated to Illumina sequencing adapters. The ligation products were size selected by agarose gel electrophoresis, PCR amplified, and sequenced using Illumina Novaseq6000 by Gene *Denovo* Biotechnology Co. (Guangzhou, China).

RNA sequencing data analysis

Differentially expressed genes (DEGs) were assessed by analysis of differential RNA expression between two groups. Transcripts with the parameter of a p value below 0.05 and an absolute fold change of 1.5 or greater were considered differentially expressed. Gene Ontology (GO) analysis was performed using the GO database. The calculated p value was FDR corrected, with an FDR of 0.05 or less as the threshold. Bioinformatic analysis was performed using a real-time interactive online platform for data analysis (http://www.omicsmart.com).

Quantitative Real-Time PCR (qRT-PCR)

qRT-PCR was conducted to measure the expression of differentially expressed mRNA. The 12 mice were randomly divided into 4 groups, and the modeling mentioned above was employed to administer different stimuli to each group. Immediately after the stimulation, the mice were euthanized to obtain hippocampal tissue. Hippocampal RNA was extracted using a TSINGKE TSP413 RNAprep FastPure kit (Beijing Tsingke Biotechnology Co., Ltd.). Target genes were reverse transcribed and amplified using MightyScript First Strand cDNA Synthesis Master Mix (Sangon, Shanghai, China) according to the manufacturer's instructions. Quantitative real-time PCR was performed with the LightCycler 480 (Roche, Rotkreuz, Switzerland) and SYBR Green PCR master mix (Yeasen, Shanghai, China). The fold change in the gene expression was calculated using the comparative Ct method, and three replicates were tested for each cDNA sample. The following primers were used (synthesized by Tsingke Biotechnology Co.): Slc17a6; 5′- GTCGGTAAAACAAAGGATTTTGGC -3′ (forward), 5′- GCTTCTTCTCCAGCACCCTGTA -3′ (reverse) and β-actin; 5′-AACAGTCCGCCTAGAAGCAC-3′ (forward), 5′-CGTTGACATCCGTAAAGACC-3′ (reverse). Gene expression levels were normalized to those of β-actin as an endogenous control. Each experiment was repeated at least three times.

QUANTIFICATION AND STATISTICAL ANALYSIS

The results are presented as the mean ± SEM. Rectal temperature change, arterial blood pressure, behavioral experiment indices, hippocampal region immunofluorescence staining intensity, and mRNA relative expression levels were subjected to statistical analysis using one-way analysis of variance. Tukey's test was used to compare all the groups. Differences were considered statistically significant at $p < 0.05$. Statistical analyses were performed using GraphPad Prism 9.5 (Insightful Science, CA, USA).